Magnetoabsorption of large bipolarons

J. T. Devreese* and V. M. Fomin†
Universitaire Instelling Antwerpen, Departement Natuurkunde, Universiteitsplein 1, B-2610 Antwerpen-Wilrijk, Belgium
(Received 12 March 1996)

The magnetoabsorption of large bipolarons is investigated using the path-integral method. The response of a bipolaron in a magnetic field to an external electromagnetic field is derived from a generalized anisotropic modeling influence phase in the framework of the memory-function approach. The resulting magnetoabsorption spectrum of large bipolarons is presented for several values of the magnetic field. A general feature is that this spectrum consists of a series of relatively narrow peaks. The peculiarities of the magnetoabsorption spectrum of the bipolaron as a function of the frequency of the electromagnetic field are attributed to the transitions involving scattering states of a bipolaron. The shape of the magnetoabsorption spectrum, due to free polarons at lower magnetic fields, drastically changes at higher magnetic fields where bipolarons are stable. [S0163-1829(96)03429-7]

I. INTRODUCTION

The transport properties of polar and ionic solids are substantially influenced by the polaron coupling. Large polarons have been most clearly manifested by investigations of their properties in magnetic fields (see the recent review on polarons in Ref. 1).

Feynman, Hellwarth, Iddings, and Platzman[2] (FHIP) have elaborated a framework allowing the analysis of the response properties of a polaron to a constant electric field (the mobility) and to an electromagnetic field (the impedance function of its frequency ω), using a path-integral polaron model.[3] This result and related approximations allowed one to explain the experimental results of Brown and co-workers[4] on alkali halides and silver halides, in the temperature region where the electron–LO-phonon scattering is the dominant process (at low temperatures $T<50$ K the impurity scattering starts to prevail). It was shown in Ref. 5 how the optical absorption of Fröhlich polarons, for all coupling, can be calculated starting from the FHIP scheme. The weak-coupling limit of the obtained absorption coefficient coincides with the results by Gurevich *et al.*,[6] whereas the structure of the strong-coupling limit confirms the identification of the internal polaron excitations by Kartheuser *et al.*[7]

Larsen[8,9] has made important contributions to the theoretical study of polarons in magnetic fields. In particular, he pointed out the level repulsion close to the crossing of levels at $\omega_c=\omega_{\rm LO}$ (ω_c is the cyclotron resonance frequency, while $\omega_{\rm LO}$ is the frequency of longitudinal optical phonons) and the pinning of Landau levels to the phonon continuum as $\omega_c\rightarrow\infty$. The first indications for these phenomena were provided by measurements on InSb (Ref. 10) and CdTe.[11] Detailed line shape studies for the weak coupling of the cyclotron resonance, revealing a double-peak structure close to $\omega_c=\omega_{\rm LO}$, were displayed by Vigneron *et al.*[12] and independently in Refs. 13,14.

In Ref. 15, the Feynman model of the polaron was generalized to the case where a static external magnetic field was applied. A quadratic, retarded model interaction was introduced to simulate the polaron (retarded Coulomb) interaction and, in analogy to the zero-magnetic-field case, the Jensen-Feynman inequality was used as a working hypothesis. Most of the existing theories of polarons in a magnetic field (developed by Hellwarth and Platzman,[16] Marshall and Chawla,[17] Evrard *et al.*,[18] and Lépine and Matz[19]) are obtained as special cases of the results of Ref. 15. A question of considerable significance concerns the validity of the Jensen-Feynman inequality in the presence of a magnetic field (see Refs. 20,21, Sec. 3.4 in Ref. 22 and Ref. 9 for the details). A generalization of the Jensen-Feynman inequality, which remains valid in the case of a nonzero magnetic field, was derived in Ref. 23. The conditions were determined to be imposed on the variational parameters in the trial action, so that the Jensen-Feynman inequality for a polaron in a magnetic field remains valid. The magnetoabsorption of polarons analyzed compehensively in Ref. 24, both numerically and analytically in a variety of limiting cases, leads to the best quantitative agreement between theory and the more recent precise cyclotron mass measurements in AgBr and AgCl by Hodby *et al.*.[25] Like in the work in three dimensions (3D), the theory of cyclotron resonance in the two-dimensional electron gas (2DEG), for cases where the electron-phonon interaction plays a significant role,[26] is formulated using the memory-function formalism.

A nice example, clearly demonstrating the polaron coupling, is provided by the cyclotron resonance in the 2DEG which naturally occurs in InSe where $\alpha\approx 0.3$.[27] Polaron cyclotron resonance has even been observed up to 220 K in n-type ZnS by Miura *et al.*[28] A quantitative interpretation of the cyclotron resonance measurements in n-GaAs and AlGaAs-GaAs heterojunctions was obtained on the basis of the polaron theory taking into account three factors: dimensionality, band nonparabolicity, and screening.[29] Impurity-bound resonant magnetopolarons have been clearly observed in bulk GaAs and GaAs-$Al_xGa_{1-x}As$ multiple quantum wells.[30]

When two electrons (or two holes) interact with each other simultaneously through the Coulomb force and via the electron-phonon interaction either two independent polarons can occur or a bound state of two polarons — the *bipolaron*

— can arise (see Refs. 31–36 on large bipolarons and a compehensive review in Ref. 37 concerning small bipolarons). Whether bipolarons are stable or not, depends on the competition between the repulsive forces (direct Coulomb interaction) and the attractive forces (mediated through the electron-phonon interaction). Verbist *et al.*[34,35] analyzed the large bipolaron using the Feynman path-integral formalism. They introduced a ''phase diagram'' for the polaron-bipolaron system on the basis of a generalization of Feynman's trial action and showed that a Fröhlich coupling constant as high as 6.8 is needed in 3D to allow for bipolaron formation. In Refs. 34,35 it was shown furthermore that the large bipolaron formation is facilitated in 2D as compared to 3D. Experimental evidence for bipolarons, e.g., from the data on magnetization and electric conductivity in Ti_4O_7, as well as in $Na_{0.3}V_2O_5$ and polyacetylene, is discussed by Mott.[38]

The optical and kinetic properties of polar and ionic solids are influenced by the polaron coupling. There has been an ongoing interest in the optical properties of large polarons.[6,2,7,5] Large polaron effects have been most clearly revealed by investigations in magnetic fields.[8,24,9] In the framework of the renewed interest in bipolaron theory,[31–34,36,37] an analysis of the absorption of large bipolarons without a magnetic field was given recently.[39] The present paper (see also Ref. 40) provides an investigation of the optical absorption spectrum of large bipolarons in a magnetic field.

For this purpose, we have applied the method proposed to describe transport phenomena by Thornber and Feynman[41,42] in the framework of the path-integral formalism (see also an alternative derivation in Ref. 43), which was generalized and used in Ref. 22 to investigate nonequilibrium and nonlinear properties of polarons. In what follows we confine ourselves to the spin-singlet states of a bipolaron. A variational treatment of both spin-singlet and spin-triplet states of large bipolarons (in 2D) and for sufficiently strong coupling in high magnetic fields has been presented elsewhere.[44] The starting point for the present study is the treatment of a bipolaron in a magnetic field recently developed in Ref. 45 within the framework of the path-integral theory for all values of the Pekar-Fröhlich coupling constant and for all magnetic field strengths. The path-integral approach for a bipolaron[34] was generalized to the case of a bipolaron in a magnetic field. It was demonstrated in Ref. 45, that the magnetic field favors bipolaron formation.

II. PATH-INTEGRAL APPROACH

The Lagrangian of a bipolaron subjected to an electromagnetic field $\mathbf{E}(t)$ (which will be considered in the dipole approximation) and to a constant magnetic field $\mathbf{B}=(0,0,B)$ is

$$\mathcal{L}=\mathcal{L}_c(\mathbf{r}_1,\mathbf{r}_2,\dot{\mathbf{r}}_1,\dot{\mathbf{r}}_2,t)+\mathcal{L}_p+\mathcal{L}_{c-p}, \tag{1}$$

where the electrons, the phonon field and the electron-phonon interaction are described by the Lagrangians

$$\mathcal{L}_c(\mathbf{r}_1,\mathbf{r}_2,\dot{\mathbf{r}}_1,\dot{\mathbf{r}}_2,t)=\sum_{n=1,2}\left[\frac{m_b\dot{\mathbf{r}}_n^2}{2}+\frac{e}{c}\mathbf{r}\cdot\mathbf{A}(\mathbf{r}_n)-e\mathbf{r}_n\cdot\mathbf{E}(t)\right]$$

$$-U(\mathbf{r}_1-\mathbf{r}_2), \tag{2}$$

$\mathcal{L}_p$ and $\mathcal{L}_{c-p}$, respectively. Here m_b denotes the electron band mass; the vector potential describing the magnetic field in the Coulomb gauge is $\mathbf{A}(\mathbf{r})=(B/2)(-y,x,0)$ and the potential energy of the Coulomb repulsion is $U(\mathbf{r})=U/|\mathbf{r}|$ with $U\equiv e^2/\varepsilon_\infty$.

The matrix elements of the nonstationary statistical operator of a singlet state of a bipolaron can be represented as[22]

$$\langle\mathbf{r}_1,\mathbf{r}_2|\rho_c[t,t_0,\rho_c(t_0)]|\mathbf{r}_1',\mathbf{r}_2\rangle=\int d\mathbf{r}_{10}d\mathbf{r}_{20}d\mathbf{r}_{10}'d\mathbf{r}_{20}'G(\mathbf{r}_1,\mathbf{r}_2,\mathbf{r}_1',\mathbf{r}_2';t|\mathbf{r}_{10},\mathbf{r}_{20},\mathbf{r}_{10}',\mathbf{r}_{20}';t_0)\langle\mathbf{r}_{10},\mathbf{r}_{20}|\rho_c(t_0)|\mathbf{r}_{10}',\mathbf{r}_{20}'\rangle, \tag{3}$$

where the propagator is a multiple Feynman path integral over the paths $\mathbf{r}_n(u), n=1,2,$ of both electrons,

$$G(\mathbf{r}_1,\mathbf{r}_2,\mathbf{r}_1',\mathbf{r}_2';t|\mathbf{r}_{10},\mathbf{r}_{20},\mathbf{r}_{10}',\mathbf{r}_{20}';t_0)=\int_{\mathbf{r}_{10}}^{\mathbf{r}_1}\int_{\mathbf{r}_{10}'}^{\mathbf{r}_1'}\int_{\mathbf{r}_{20}}^{\mathbf{r}_2}\int_{\mathbf{r}_{20}'}^{\mathbf{r}_2'}\prod_{n=1}^{2}\mathcal{D}\mathbf{r}_n(u)\mathcal{D}\mathbf{r}_n\prime(u)\exp\left\{\frac{i}{\hbar}\int_{t_0}^{t}[\mathcal{L}_c(\mathbf{r}_1(u),\mathbf{r}_2(u),\dot{\mathbf{r}}_1(u),\dot{\mathbf{r}}_2(u),u)\right.$$

$$\left.-\mathcal{L}_c(\mathbf{r}_1'(u),\mathbf{r}_2'(u),\dot{\mathbf{r}}_1'(u),\dot{\mathbf{r}}_2'(u),u)]du+\Phi_p[\mathbf{r}_1(u),\mathbf{r}_2(u),\mathbf{r}_1'(u),\mathbf{r}_2'(u),t,t_0]\right\}, \tag{4}$$

and $\rho_c(t_0)$ is the initial statistical operator of the electron subsystem. The phonon influence phase Φ_p describes a retarded interaction between electrons ($n' \neq n$) or a retarded self-interaction of each electron ($n'=n$) due to the elimination of the phonon coordinates. It is given by

$$\Phi_p[\mathbf{r}_1(u),\mathbf{r}_2(u),\mathbf{r}_1'(u),\mathbf{r}_2'(u),t,t_0] = -\sum_{n,n'=1}^{2}\sum_{\mathbf{k}}\frac{|V_k|^2}{\hbar^2}\int_{t_0}^{t}du\int_{t_0}^{u}du'[e^{i\mathbf{k}\cdot\mathbf{r}_n(u)}-e^{i\mathbf{k}\cdot\mathbf{r}_{n'}(u)}] \times[T^*_{\omega_k}(u-u')e^{-i\mathbf{k}\cdot\mathbf{r}_{n'}(u')}-T_{\omega_k}(u-u')e^{-i\mathbf{k}\cdot\mathbf{r}'_{n'}(u')}]. \tag{5}$$

As is well known, the Fourier coefficient of the interaction potential between an electron and the longitudinal optical phonons of wave vector $\mathbf{k}$ and frequency $\omega_k \equiv \omega_{\mathrm{LO}}$, for a three-dimensional system of volume V, is

$$V_k = -i\frac{\hbar\omega_{\mathrm{LO}}}{k}\left(\frac{4\pi\alpha}{V}\right)^{1/2}\left(\frac{\hbar}{2m_b\omega_{\mathrm{LO}}}\right)^{1/4}, \tag{6}$$

with the Pekar-Fröhlich coupling constant

$$\alpha = \frac{e^2}{\hbar c}\sqrt{\frac{m_b c^2}{2\hbar\omega_{\mathrm{LO}}}}\left(\frac{1}{\varepsilon_\infty}-\frac{1}{\varepsilon_0}\right), \tag{7}$$

determined by the optical (ε_∞) and statical (ε_0) dielectric constants of the polar crystal. The memory function in Eq. (5) in case of an equilibrium distribution is

$$T_{\omega_k}(u) = \frac{\cos[i\omega_k(u-i\hbar\beta/2)]}{\sinh[\hbar|\omega_k|\beta/2]}, \quad \beta = \frac{1}{k_B T}. \tag{8}$$

Note that in the zero-temperature limit it follows that

$$\lim_{\beta\to\infty} T_{\omega_k}(u) = e^{i|\omega_k|u}. \tag{9}$$

The average kinetic momentum $\langle\mathbf{P}(t)\rangle$ of the two-electron system as a whole is governed by the equation of motion

$$\frac{d\langle\mathbf{P}(t)\rangle}{dt} = -2e\mathbf{E}(t) - \frac{e}{m_b c}[\langle\mathbf{P}(t)\rangle,\mathbf{B}] + \left.\frac{\partial\langle\mathbf{P}(t)\rangle}{\partial t}\right|_{e\text{-}p}, \tag{10}$$

where the last term in the right-hand side is the ''collision integral'' due to the electron-phonon interaction. Next we perform a change of variables to a new frame of reference,

$$\mathbf{r}_n(u) = \mathbf{R}(u) + \vec{\rho}(u), \quad \mathbf{r}'_n(u) = \mathbf{R}(u) + \vec{\rho}'(u), \tag{11}$$

and assume a steady state of the system[41,22] ($t_0 \to -\infty$). In this case all operations in Eq. (3) concerning the initial state are irrelevant, and the equation of motion for the vector function $\mathbf{R}(t)$, which is connected to the average kinetic momentum as $\langle\mathbf{P}(t)\rangle = 2m_b\dot{\mathbf{R}}(t)$, takes the form

$$m_b\frac{d^2\mathbf{R}(t)}{dt^2} + e\mathbf{E}(t) + \frac{e}{c}\left[\frac{d\mathbf{R}(t)}{dt},\mathbf{B}\right] = \mathbf{F}(t), \tag{12}$$

where the force due to the electron-phonon interaction,

$$\mathbf{F}(t) = \mathrm{Re}\sum_{n,n'=1}^{2}\sum_{\mathbf{k}}\frac{|V_k|^2\mathbf{k}}{\hbar} \times\int_{-\infty}^{t}dt' T_{\omega_{\mathrm{LO}}}(t-t')e^{i\mathbf{k}\cdot[\mathbf{R}(t)-\mathbf{R}(t')]} \times\langle e^{i\mathbf{k}\cdot[\vec{\rho}_n(t)-\vec{\rho}'_{n'}(t')]}\rangle_p, \tag{13}$$

is expressed in terms of the correlation functions

$$\langle e^{i\mathbf{k}\cdot[\vec{\rho}_n(t)-\vec{\rho}'_{n'}(t')]}\rangle_p \equiv \int d\vec{\rho}_1 d\vec{\rho}_2 d\vec{\rho}_{10} d\vec{\rho}_{20} d\vec{\rho}'_{10} d\vec{\rho}'_{20}\int_{\vec{\rho}_{10}}^{\vec{\rho}_1}\int_{\vec{\rho}'_{10}}^{\vec{\rho}_1}\int_{\vec{\rho}_{20}}^{\vec{\rho}_2}\int_{\vec{\rho}'_{20}}^{\vec{\rho}_2}\prod_{n=1}^{2}\mathcal{D}\vec{\rho}_n(u)\mathcal{D}\vec{\rho}'_{n'}(u) \times\exp\left\{\frac{i}{\hbar}\int_{t_0}^{t}[\mathcal{L}_c(\vec{\rho}_1(u),\vec{\rho}_2(u),\dot{\vec{\rho}}_1(u),\dot{\vec{\rho}}_2(u),u)-\mathcal{L}_c(\vec{\rho}'_1(u),\vec{\rho}'_2(u),\dot{\vec{\rho}}'_1(u),\dot{\vec{\rho}}'_2(u),u)]du + \Phi_p[\vec{\rho}_1(u),\vec{\rho}_2(u),\vec{\rho}'_1(u),\vec{\rho}'_2(u),t,t_0]\right\} e^{i\mathbf{k}\cdot[\vec{\rho}_n(t)-\vec{\rho}'_{n'}(t')]}\langle\vec{\rho}_{10},\vec{\rho}_{20}|\rho_c(t_0)|\vec{\rho}'_{10},\vec{\rho}'_{20}\rangle. \tag{14}$$

III. CORRELATION FUNCTIONS

In order to obtain the force given by Eq. (13), we approximate the dynamics described by Eq. (14) by that corresponding to the modeling of the electron-phonon interaction by an interaction of two electrons with two fictitious particles as recently derived in Ref. 45 (see also Ref. 46):

$$\mathbf{F}(t) = \mathrm{Re}\sum_{n,n'=1}^{2}\sum_{\mathbf{k}}\frac{|V_k|^2\mathbf{k}}{\hbar} \times\int_{-\infty}^{t}dt' T_{\omega_{\mathrm{LO}}}(t-t')e^{i\mathbf{k}\cdot[\mathbf{R}(t)-\mathbf{R}(t')]} \times\langle e^{i\mathbf{k}\cdot[\vec{\rho}_n(t)-\vec{\rho}'_{n}(t')]}\rangle_M, \tag{15}$$

where the correlation functions $\langle e^{i\mathbf{k}\cdot[\vec{\rho}_n(t)-\vec{\rho}'_{n'}(t')]}\rangle_M$ differ from expression (14) because of the substitution of the exact influence phase (5) by the model influence phase Φ_M. Since the motions perpendicular and parallel to the z axis are independent, the correlation functions decouple:

$$\langle e^{i\mathbf{k}\cdot[\vec{\rho}_n(t)-\vec{\rho}'_{n'}(t')]}\rangle_M = \langle e^{i\mathbf{k}_\perp\cdot[\vec{\rho}_n(t)-\vec{\rho}'_{n'}(t')]}\rangle_M \langle e^{i\mathbf{k}_\parallel\cdot[\vec{\rho}_n(t)-\vec{\rho}'_{n'}(t')]}\rangle_M , \tag{16}$$

with $\mathbf{k}_\perp = k_x\mathbf{e}_x + k_y\mathbf{e}_y$, $\mathbf{k}_\parallel = k_z\mathbf{e}_z$. After introducing the normal coordinates,[45] the correlation functions entering (16) take the form

$$\langle e^{i\mathbf{k}_\perp\cdot[\vec{\rho}_n(t)-\vec{\rho}'_{n'}(t')]}\rangle_M = \left\langle \exp\left\{ i\frac{k_x}{2}[X(t)-X'(t')] + i\frac{k_y}{2}[Y(t)-Y'(t')]\right\}\right\rangle_M \times \left\langle \exp\left\{ (-1)^{n-1}\left[i\frac{k_x}{2}[x(t)-(-1)^{n'-1}x'(t')] + i\frac{k_y}{2}[y(t)-(-1)^{n'-1}y'(t')]\right]\right\}\right\rangle_M . \tag{17}$$

The generating functional of real-time correlation functions for an equilibrium ensemble of the normal excitation modes with eigenfrequency ω described by a statistical operator $\rho_{\mathrm{eq}}(t_0)$, is given by[41,22]

$$\left\langle \exp\left\{ i\int_{t_0}^{t} du[\chi(u)b(u)+b^\dagger(u)\gamma(u)]\right\}\exp\left\{ i\int_{t_0}^{t} du[\chi'(u)b'(u)+b'^\dagger(u)\gamma'(u)]\right\}\right\rangle_M$$
$$\equiv \mathrm{Tr}\mathcal{T}\exp\left\{ i\int_{t_0}^{t} du[-b^\dagger(u)\omega b(u)+\chi(u)b(u)+b^\dagger(u)\gamma(u)]\right\}\rho_{\mathrm{eq}}(t_0)\mathcal{T}'^{-}\left\langle \exp\left\{ i\int_{t_0}^{t} du[b'^\dagger(u)\omega b'(u) + \chi'(u)b'(u)+b'^\dagger(u)\gamma'(u)]\right\}\right\rangle_M$$
$$= \exp\left\{ -\int_{t_0}^{t} du\int_{t_0}^{u} du'[\chi'(u)+\chi(u)][T_\omega(u-u')\gamma'(u')+T_\omega(u'-u)\gamma(u')]\right\}, \tag{18}$$

where $\mathcal{T}$ is the chronological-ordering operator and $\mathcal{T}'^{-}$ is the antichronological-ordering operator which acts on the primed operators. After rather lengthy algebra, this gives the final result in a remarkably compact form:

$$\langle e^{i\mathbf{k}_\perp\cdot[\vec{\rho}_n(t)-\vec{\rho}'_{n'}(t')]}\rangle_M = \langle e^{i\mathbf{k}_\perp\cdot[\vec{\rho}_{n'}(t)-\vec{\rho}'_{n'}(t')]}\rangle_M = e^{-k_\perp^2 D(t-t')}, \tag{19}$$

$$D(t-t') \equiv \frac{1}{4}\left\{ \sum_{j=1}^{7} \lambda_j^2[T_{s_j}(0)-\sigma_j(n,n')T_{s_j}(t-t')]\right\}, \tag{20}$$

$$\langle e^{i\mathbf{k}_\parallel\cdot[\vec{\rho}_n(t)-\vec{\rho}'_{n'}(t')]}\rangle_M = \langle e^{i\mathbf{k}_\parallel\cdot[\vec{\rho}_{n'}(t)-\vec{\rho}'_{n'}(t')]}\rangle_M = e^{-k_z^2 F(t-t')}, \tag{21}$$

$$F(t-t') = \frac{1}{4}\left\{ -i(t-t')\frac{\hbar W^2}{m_b\Omega_1^2} + 2\sum_{J=1}^{3}\Lambda_J^2[T_{\Omega_J}(0)-\Sigma_J(n,n')T_{\Omega_J}(t-t')]\right\}, \tag{22}$$

$$\sigma_j(n,n') = \begin{cases} 1 & \text{if } j=1,2,3, \\ 1 & \text{if } j=4,5,6,7 \text{ and } n=n', \\ -1 & \text{if } j=4,5,6,7 \text{ and } n\neq n', \end{cases} \tag{23}$$

$$\Sigma_J(n,n') = \begin{cases} 1 & \text{if } J=1, \\ 1 & \text{if } J=2,3 \text{ and } n=n', \\ -1 & \text{if } J=2,3 \text{ and } n\neq n'. \end{cases} \tag{24}$$

The denotations for the eigenfrequencies s_j, $j=1,\ldots,7$, and Ω_J, $J=1,2,3$, and for the corresponding coefficients λ_j and Λ_J are the same as in Ref. 45. The modes s_j, $j=1,\ldots,3$, and Ω_J, $J=1,2$, describe the center-of-mass motion of a bipolaron in the xy plane and along the z axis, respectively, while the modes s_j, $j=4,\ldots,7$, and Ω_3 describe the relative motions in a bipolaron. The motions of electrons and fictitious particles in the xy plane, corresponding to the normal modes with frequencies s_j, $j=1,\ldots,7$, of a large-bipolaron model,[45] are schematically represented in Fig. 1. Note that the amplitudes of the fictitious particles for the realistic values of parameters are two orders of magnitude smaller than those of the electrons, and are considerably magnified in this figure.

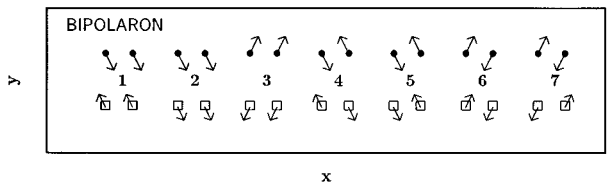

FIG. 1. Scheme of the motions of electrons (denoted as ●) and fictitious particles (□) in the xy plane, corresponding to the normal modes with frequencies s_j, $j=1,\ldots,7$, of a large bipolaron model (Ref. 45). The amplitudes of the fictitious particles, which for the realistic parameters are two orders of magnitude smaller than those of electrons, are shown magnified.

IV. RESPONSE OF A BIPOLARON IN A MAGNETIC FIELD

Within the framework of linear-response theory, the expansion of the force (15) to first order in $\mathbf{R}(t)$ gives

$$\mathbf{F}(t)=-\int_0^\infty dt''\ \mathrm{Im}\{T_{\omega_{\mathrm{LO}}}(t'')\overleftrightarrow{\mathbf{S}}(t'')\}\cdot[\mathbf{R}(t)-\mathbf{R}(t-t'')], \tag{25}$$

with

$$\overleftrightarrow{\mathbf{S}}(t'')=\sum_{n,n'=1}^{2}\sum_{\mathbf{k}}\frac{|V_k|^2\mathbf{k})(\mathbf{k}}{\hbar}\langle e^{i\mathbf{k}\cdot[\vec{\rho}_n(t)-\vec{\rho}'_{n'}(t-t'')]}\rangle_M . \tag{26}$$

Performing now the Fourier analysis of Eq. (12), we find the dielectric permittivity at the frequency ω to be

$$\overleftrightarrow{\varepsilon}(\omega)=-2e^2\left[m_b\omega^2\overleftrightarrow{\mathbf{I}}-i\frac{e}{c}\omega\overleftrightarrow{\mathbf{B}}-\overleftrightarrow{\mathbf{T}}(\omega)\right]^{-1}, \tag{27}$$

where $\overleftrightarrow{\mathbf{I}}$ is the unit tensor, $\overleftrightarrow{\mathbf{B}}\cdot\mathbf{v}\equiv[\mathbf{B},\mathbf{v}]$, and the *memory tensor* is defined as

$$\overleftrightarrow{\mathbf{T}}(\omega)=\int_0^\infty dt'(1-e^{i\omega t'})\ \mathrm{Im}\{T_{\omega_{\mathrm{LO}}}(t')\overleftrightarrow{\mathbf{S}}(t')\}. \tag{28}$$

The numerical analysis has shown that (26) is an oscillating function of time. Therefore, in order to investigate its Fourier spectrum, it is convenient to expand the correlation functions (20) and (22) in powers of the oscillating exponentials entering the functions $T_{s_j}(t'),T_{\Omega_J}(t')$, namely,

$$e^{-k_\perp^2 D(t-t')}=e^{-k_\perp^2\overline{D}}\left\{\prod_{j=1}^{7}\sum_{n_j=0}^{\infty}\right\}\prod_{j=1}^{7}\left[\frac{k_\perp^2\sigma_j(n,n')\lambda_j^2}{4\overline{D}}\times T_{s_j}(t-t')\right]^{n_j}, \tag{29}$$

$$\overline{D}\equiv\frac{1}{4}\left[\sum_{j=1}^{7}\lambda_j^2 T_{s_j}(0)\right], \tag{30}$$

$$e^{-k_z^2 F(t-t')}=e^{-k_z^2[\overline{F}-(1/4)i(t-t')\hbar W^2/m_b\Omega_1^2]}\times\left\{\prod_{J=1}^{3}\sum_{N_J=0}^{\infty}\right\}\prod_{J=1}^{3}\left[\frac{k_z^2\Sigma_J(n,n')\Lambda_J^2}{2\overline{F}}\times T_{\Omega_J}(t-t')\right]^{N_J}, \tag{31}$$

$$\overline{F}=\frac{1}{2}\left[\sum_{J=1}^{3}\Lambda_J^2 T_{\Omega_J}(0)\right]. \tag{32}$$

Then the integration with respect to time in the memory tensor (28) is performed analytically. Introducing a shorthand denotation

$$\sum_{\{n,N\}}\equiv\left\{\prod_{j=1}^{7}\sum_{n_j=0}^{\infty}\right\}\left\{\prod_{J=1}^{3}\sum_{N_J=0}^{\infty}\right\}, \tag{33}$$

we represent the result in the form

$$T^M(\pm\omega)=\frac{\alpha\omega_{\mathrm{LO}}^2 m_b C}{2\sqrt{2}\pi\overline{D}\sqrt{\overline{F}}}\sum_{n,n'=1}^{2}\sum_{\{n,N\}}\left(\sum_{j=1}^{7}n_j\right)\prod_{j=1}^{7}\left(\frac{\sigma_j(n,n')\lambda_j^2}{4\overline{D}}\right)^{n_j}\prod_{J=1}^{3}\left(\frac{\Sigma_J(n,n')\Lambda_J^2}{2\overline{F}}\right)^{N_J}$$
$$\times\left\{\int_0^\infty d\zeta e^{-\zeta}\zeta\sum_{J=1}^{3}N_J^{-1/2}\left[\frac{\mathcal{P}}{C(1+\Sigma_{j=1}^{7}n_j+\Sigma_{J=1}^{3}N_J)+\zeta}-\frac{\mathcal{P}}{C(1\pm\omega+\Sigma_{j=1}^{7}n_j+\Sigma_{J=1}^{3}N_J)+\zeta}\right]\right.$$
$$+i\pi\Theta\left[-\left(1\pm\omega+\sum_{j=1}^{7}n_j+\sum_{J=1}^{3}N_J\right)\right]\exp\left[C\left(1\pm\omega+\sum_{j=1}^{7}n_j+\sum_{J=1}^{3}N_J\right)\right]$$
$$\left.\times\left[-C\left(1\pm\omega+\sum_{j=1}^{7}n_j+\sum_{J=1}^{3}N_J\right)\right]^{\sum_{J=1}^{3}N_J-1/2}\right\}, \tag{34}$$

$$T_{\parallel}^{M}(\pm\omega)=\frac{\alpha\omega_{\mathrm{LO}}^{2}m_{b}C}{2\sqrt{2}\,\pi\overline{F}^{3/2}}\sum_{n,n'=1}^{2}\sum_{\{n,N\}}\prod_{j=1}^{7}\left(\frac{\sigma_{j}(n,n')\lambda_{j}^{2}}{4\overline{D}}\right)^{n_{j}}\prod_{J=1}^{3}\left(\frac{\Sigma_{J}(n,n')\Lambda_{J}^{2}}{2\overline{F}}\right)^{N_{J}}$$

$$\times\left\{\int_{0}^{\infty}d\zeta E_{\sum_{j=1}^{7}n_{j}}\left(\frac{\overline{D}}{\overline{F}}\zeta\right)e^{-\zeta}\zeta^{\sum_{J=1}^{3}N_{J}+1/2}\left[\frac{\mathcal{P}}{C(1+\Sigma_{j=1}^{7}n_{j}+\Sigma_{J=1}^{3}N_{J})+\zeta}-\frac{\mathcal{P}}{C(1\pm\omega+\Sigma_{j=1}^{7}n_{j}+\Sigma_{J=1}^{3}N_{J})+\zeta}\right]\right.$$

$$+i\pi\Theta\left[-\left(1\pm\omega+\sum_{j=1}^{7}n_{j}+\sum_{J=1}^{3}N_{J}\right)\right]E_{\sum_{j=1}^{7}n_{j}}\left[-\frac{\overline{D}}{\overline{F}}C\left(1\pm\omega+\sum_{j=1}^{7}n_{j}+\sum_{J=1}^{3}N_{J}\right)\right]$$

$$\left.\times\exp\left[C\left(1\pm\omega+\sum_{j=1}^{7}n_{j}+\sum_{J=1}^{3}N_{J}\right)\right]\left[-C\left(1\pm\omega+\sum_{j=1}^{7}n_{j}+\sum_{J=1}^{3}N_{J}\right)\right]^{\sum_{J=1}^{3}N_{J}+\frac{1}{2}}\right\},\tag{35}$$

$$T_{\perp}^{M}=\frac{T^{M}-T_{\parallel}^{M}}{2},\tag{36}$$

$$E_{n}(x)=\int_{0}^{\infty}d\kappa\mathrm{e}^{-\kappa}\frac{\kappa^{n}}{\kappa+x}.\tag{37}$$

Here $C=4\overline{F}\Omega_{1}^{2}/W^{2}$, $\Theta(x)$ is Heaviside function, and $\mathcal{P}$ denotes the principal value of the integral.

The resulting expression for the magneto-optical absorption obtained from the imaginary part of the dielectric permittivity (27) is, e.g., for the Faraday-active configuration

$$\varepsilon''(\omega)\sim-\frac{1}{2}\frac{\mathrm{Im}T(\omega)/\omega}{[\omega-\omega_{c}-\mathrm{Re}T(\omega)/\omega]^{2}+[\mathrm{Im}T(\omega)/\omega]^{2}},\tag{38}$$

where $\omega_{c}=eB/(m_{b}c)$ is the cyclotron frequency and $T(\omega)$ is the xx component of the memory tensor (28). This formula has been deduced and used for the investigation of the optical absorption of polarons in Ref. 5.

V. DISCUSSION OF THE MAGNETOABSORPTION SPECTRA: CONCLUSIONS

In this section the bipolaron magnetoabsorption spectrum as a function of the magnetic field is analyzed and compared with that of free polarons (see Figs. 2 to 7). Note that the case $T=0$ is considered here.

As shown in Fig. 2, at $\alpha=6.8$ and $U/\alpha=\sqrt{2}$ the ground-state energy of the bipolaron is lower than that of a system of two free polarons above a critical value of the cyclotron frequency $\omega_{c}^{\mathrm{crit}}=0.1985$. The above choice of the ratio $U/\alpha=\sqrt{2}$ is due to the fact that in the diagram representing a dimensionless ($\hbar=\omega_{\mathrm{LO}}=m_{b}=1$) repulsion U versus a coupling constant α, the line $U=\sqrt{2}\alpha$ separates the physical region $U\geqslant\sqrt{2}\alpha$ from the nonphysical one.[34,35] The subsequent figures show how the magnetoabsorption spectrum of a *bipolaron* which exists for $\omega_{c}>\omega_{c}^{\mathrm{crit}}$ changes into that specific for *free polarons*, i.e., for $\omega_{c}<\omega_{c}^{\mathrm{crit}}$.

A representative example of the magnetoabsorption spectrum of bipolarons in a magnetic field calculated from Eq. (38) for the above-mentioned parameters $\alpha=6.8$ and $U/\alpha=\sqrt{2}$ for the Faraday-active configuration at zero temperature is displayed in Figs. 3(a) and 3(b). A general feature is that this spectrum consists of a series of relatively narrow peaks reflecting the extrema of the imaginary part of the memory function represented in Fig. 3(c), which are espe-

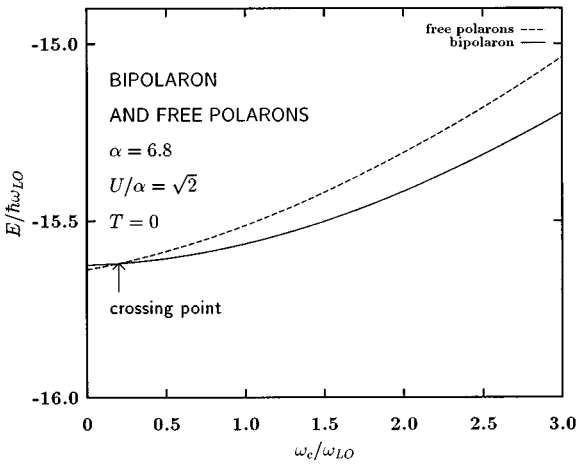

FIG. 2. Ground-state energies of a bipolaron (solid line) and of free polarons (dashed line), calculated according to the model (Ref. 45) for $\alpha=6.8$, $U/\alpha=\sqrt{2}$, and $T=0$, plotted versus a magnetic field. The point of crossing of these curves is indicated by an arrow. In the region to the right from this crossing point, a bipolaron state is the ground state of the system.

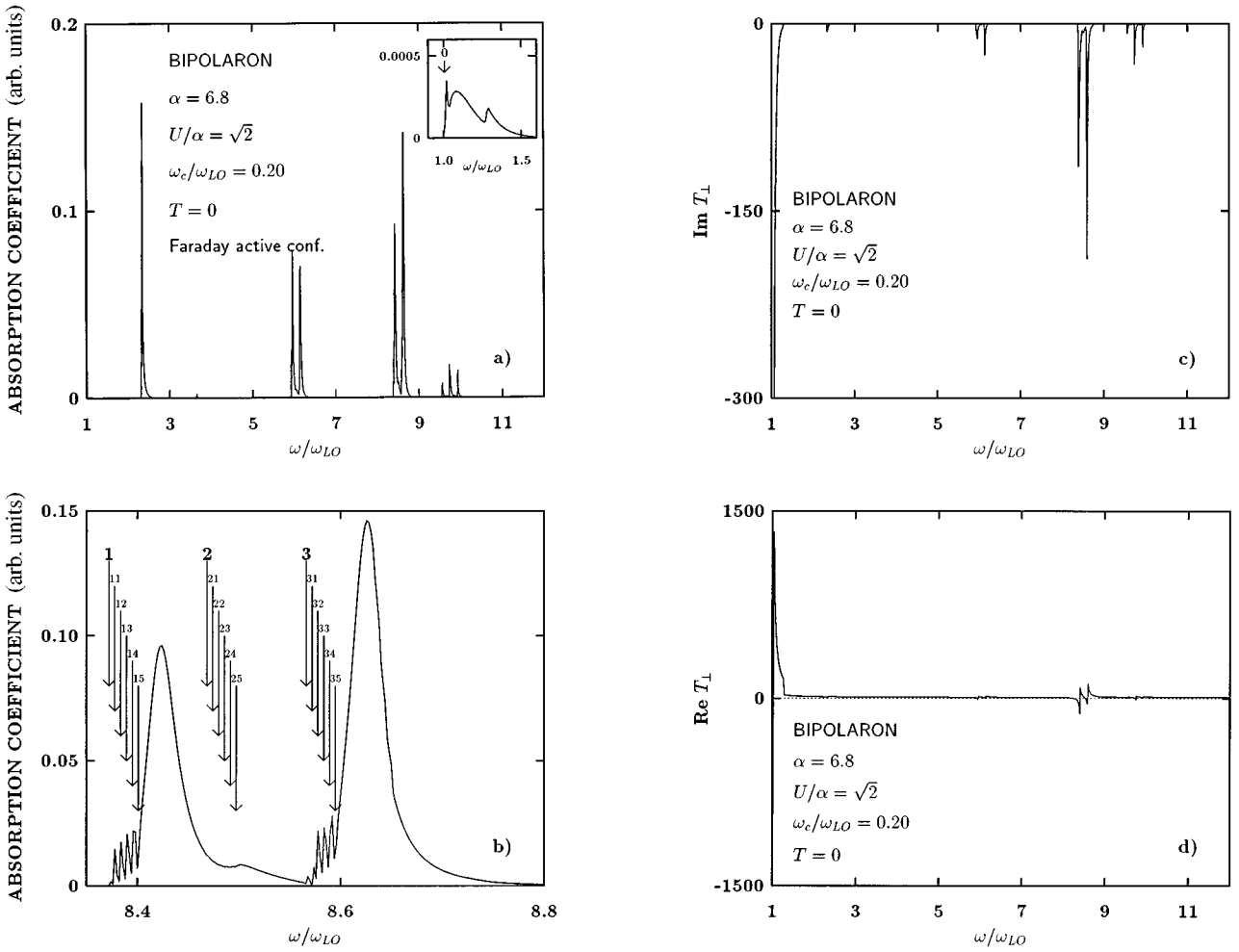

FIG. 3. Absorption spectrum of a bipolaron in a magnetic field for $\alpha=6.8$, $U/\alpha=\sqrt{2}$, and $\omega_c=0.20$ at $T=0$: a large-scale view (a) and a magnified part with the peaks having the highest oscillator strength (b) for the Faraday-active configuration; imaginary and real parts of the memory function are shown in panels (c) and (d), correspondingly. The contributions of the internal excited states of a bipolaron with $\Sigma_{j=1}^{7}|s_j|+\Sigma_{J=1}^{3}\Omega_J \leqslant 6$ are displayed. The calculation was performed with the following eigenfrequencies of a large bipolaron model (Ref. 45): $|s_1|=7.566\,24$, $|s_2|=0.005\,769\,74$, $s_3=7.372\,01$, $|s_4|=4.452\,86$, $|s_5|=0.676\,539\,4$, $s_6=0.652\,734$, $s_7=4.265\,52$, $\Omega_1=7.465\,52$, $\Omega_2=4.357\,90$, and $\Omega_3=0.659\,076$. The inset in panel (a) represents the initial part of the magnetoabsorption spectrum near $\omega/\omega_{\mathrm{LO}}=1$, where the arrow ''0'' indicates the frequency of the scattering state with one-quantum excitation of a bipolaron $1+|s_2|$. The arrows in panel (b) indicate the frequencies related to the scattering states with one-quantum excitations of a bipolaron $1+s_3$ (1), $1+\Omega_1$ (2) and $1+|s_1|$ (3) as well as with many-quantum internal excitations of a bipolaron $1+s_3+n|s_2|$ $(1n)$, $1+\Omega_1+n|s_2|$ $(2n)$, and $1+|s_1|+n|s_2|$ $(3n)$, $n=1,\ldots,5$.

cially strongly manifested in the neighborhood of the zeros of the real part of the memory function given in Fig. 3(d). [The magnetoabsorption spectrum of bipolarons for the Faraday-inactive confuguration reveals the general feature similar as for the Faraday-active configuration; cf. Figs. 5(a) and 5(b).]

This is clear from the structure of the denominator in the right-hand side of Eq. (38): $[\,\mathrm{Im}T(\omega)/\omega]/\{[\omega-\omega_c-\mathrm{Re}T(\omega)/\omega]^2+[\,\mathrm{Im}T(\omega)/\omega]^2\}$. Indeed, a specific feature of the bipolaron problem is that the values of $\mathrm{Re}T(\omega)/\omega$ are as a rule very large in comparison with the values of difference $\omega-\omega_c$ characteristic for the experimental situation. Therefore, the above expression is small in general. The physical reason of this behavior may be attributed to the fact that the *multiphonon processes* are taken into account in $T(\omega)$. For those values of the coupling constant which are relevant for the bipolaron stability region, these multiphonon processes make both real and imaginary parts of the memory tensor large. This means a shift of the resonance condition for the absorption to higher values of the frequency than the cyclotron frequency. The energy of a photon according to the respective criterion $\omega=\omega_c+\mathrm{Re}T(\omega)/\omega$ should be enough to assure not only a cyclotron transition (which would be the case in the absence of the electron-phonon interaction), but also those multiphonon transitions which are the most probable for a given value of the coupling constant.

Only in the vicinity of the zeros of the real part of the memory function (where the zero-phonon processes occur to be the most probable) does the term $[\omega-\omega_c-\mathrm{Re}T(\omega)/\omega]^2$ cease to be dominant over $[\,\mathrm{Im}T(\omega)/\omega]^2$, and hence an appreciable absorption appears in these regions. As a consequence, for a fixed value of the cyclotron frequency the resulting peaks of bipolaron absorption are separated from each other by rather large spectral intervals

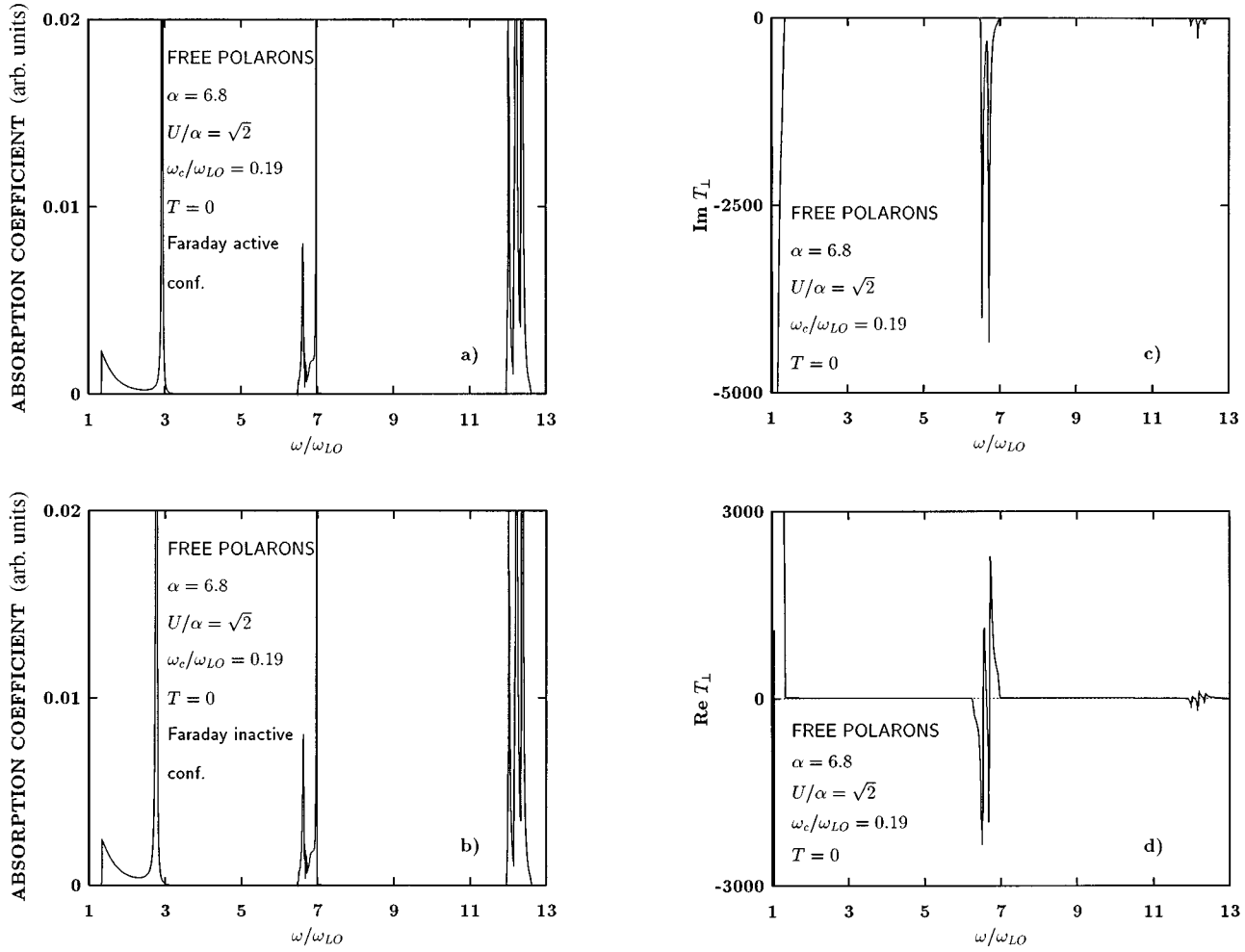

FIG. 4. Absorption spectrum of free polarons in a magnetic field for $\alpha=6.8$, $U/\alpha=\sqrt{2}$, and $\omega_c/\omega_{\mathrm{LO}}=0.19$ at $T=0$. Denotations are the same as in Fig. 3. The calculation was performed with the following eigenfrequencies of a large bipolaron model (Ref. 45): $|s_1|=|s_4|=5.65$, $|s_2|=|s_5|=0.0165$, $s_3=s_7=5.48$, $s_6\to 0$, $\Omega_1=\Omega_2=5.55$, and $\Omega_3\to 0$.

with no appreciable absorption; see, e.g., Figs. 3(a) and 3(b).

The set of quantum numbers characterizing the internal oscillatorlike excitations of a bipolaron in a magnetic field (namely, n_j, $j=1,\ldots,7$, for the eigenfrequencies s_j and N_J, $J=1,2,3$, for Ω_J, respectively) can serve as a convenient basis to classify the spectral lines related to the scattering states. The most important conclusions of the classification of the *bipolaron magnetoabsorption spectrum*, as calculated here [see, e.g., Figs. 3(a) and 3(b)], are the following.

The absorption spectral component starting at $\omega/\omega_{\mathrm{LO}}=1$ [see the inset to Fig. 3(a)] describes a sideband due to the emission of one LO phonon and is referred to the scattering states with no internal bipolaron eigenmodes excited ($\Sigma_{j=1}^{7}|s_j|+\Sigma_{J=1}^{3}\Omega_J=0$). This initial part of the bipolaron magnetoabsorption spectrum has been displayed and discussed in detail in the previous work (Ref. 40). The transitions to the scattering states of a bipolaron with the frequencies $1+n|s_2|$ involving the internal excitations of the smallest frequency ($|s_2|$) lead to a peak of absorption which is shown in the inset to Fig. 3(a). Similar to the polaronic absorption, this peak could be argued to be due to a transition into a relatively stable *relaxed excited state*[5] of a bipolaron. The broader magnetoabsorption structure revealed to the right from this peak can be probably attributed to the Franck-Condon transitions analogously to the similar structure in the case of polarons.[5] However, this analogy should be applied very cautiously because of a much more complicated energy spectrum of a magnetobipolaron as compared to a magnetopolaron.

The internal excited states of a bipolaron in a magnetic field manifest themselves first via the peculiarities of the imaginary part of the *xx* component of the memory tensor. For example, this takes place for the transitions to the scattering states with one-quantum internal excitations of a bipolaron involving four following eigenmodes describing those degrees of freedom of a bipolaron in a magnetic field which relate to the *center-of-mass motion of the bipolaron*, in the *xy* plane, $1+|s_2|=1.005\,77$ [shown by arrow ''0'' in the inset to Fig. 3(a)], $1+s_3=8.372\,01$, and $1+|s_1|=8.566\,24$ [see arrows ''1'' and ''3'' in Fig. 3(b)] as well as in the *z* direction, $1+\Omega_1=8.468\,42$ [marked by arrow ''2'' in Fig. 3(b)], due to the selection rules valid in the framework of the dipole approximation for the electromagnetic field.

Note that at the points $\omega=1+|s_j|, j=1,2,3$, the absorption according to Eq. (38) tends to zero because of the divergence of the imaginary part of the *xx* component of the memory tensor as $1/\sqrt{\omega-1-|s_j|}$. As distinct from these cases, the imaginary part of the *xx* component of the

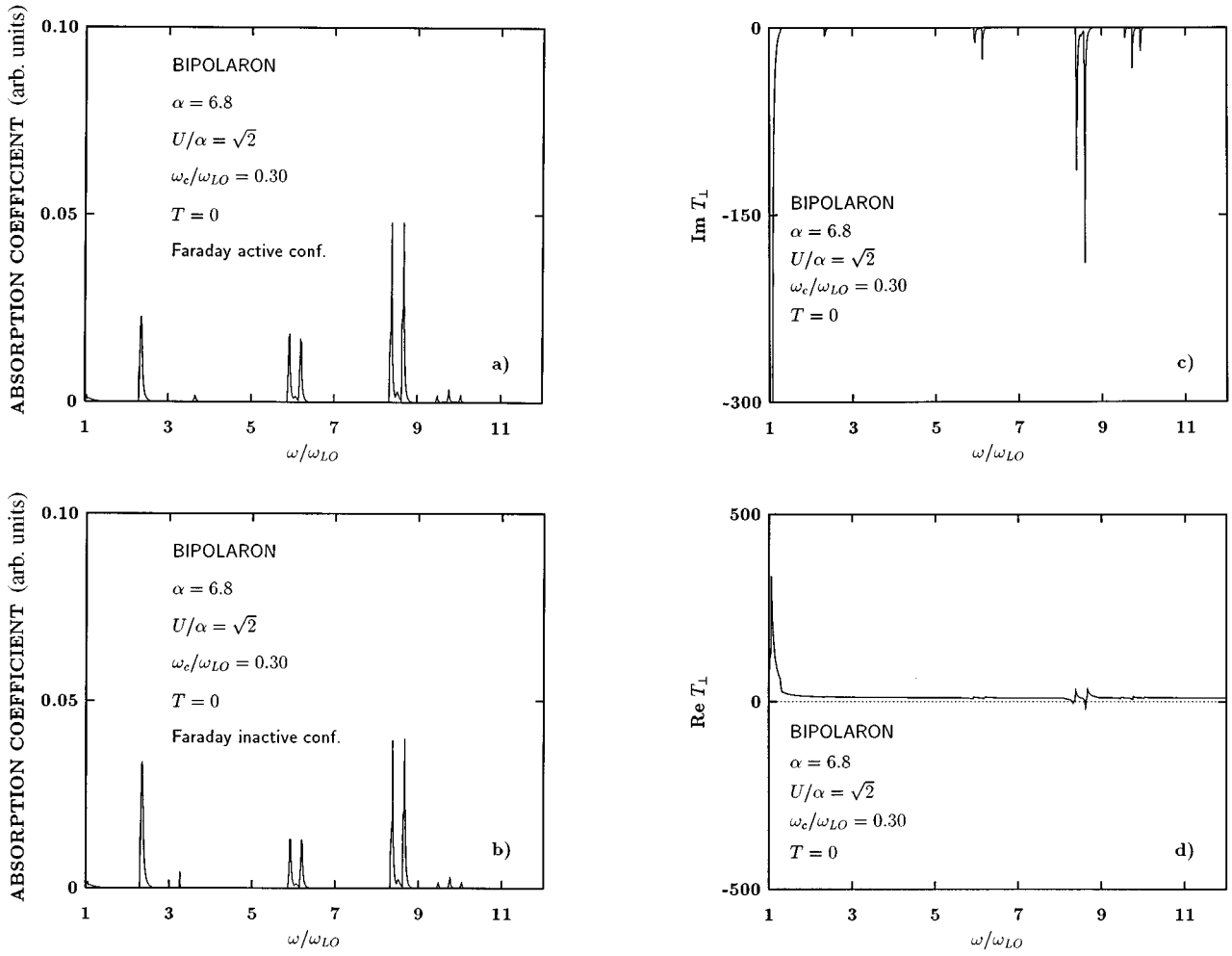

FIG. 5. Absorption spectrum of a bipolaron in a magnetic field for $\alpha=6.8$, $U/\alpha=\sqrt{2}$, and $\omega_c=0.30$ at $T=0$. Denotations are the same as in Fig. 3. The calculation was performed with the following eigenfrequencies of a large bipolaron model (Ref. 45): $|s_1|=7.620\,48$, $|s_2|=0.008\,560\,94$, $s_3=7.329\,04$, $|s_4|=4.499\,12$, $|s_5|=0.668\,715$, $s_6=0.649\,960$, $s_7=4.217\,88$, $\Omega_1=7.473\,17$, $\Omega_2=4.355\,61$, and $\Omega_3=0.659\,365$.

memory tensor tends to zero as $\sqrt{\omega-1-\Omega_1}$ for the peak related to the eigenfrequency Ω_1.

It is worth mentioning that in the above-discussed transitions to the scattering states with one-quantum internal excitations of a bipolaron, the eigenmodes related to the *relative motions* (i.e., transitions involving one of the other six eigenfrequencies, $1+|s_4|=5.452\,86$, $1+|s_5|=1.665\,394$, $1+s_6=1.652\,734$, $1+s_7=5.265\,52$, $1+\Omega_2=5.357\,90$, and $1+\Omega_3=1.659\,076$) reveal no direct contribution to the magnetoabsorption. But they play an important role in producing the combinatorial absorption peaks due to the scattering states involving many-quantum excitations of a bipolaron, as discussed below.

The scattering states due to two-quantum internal excitations of a bipolaron manifest themselves for all eigenfrequencies, because they are not subjected to selection rules similar to those which have been stated above in connection with the one-quantum excitations. E.g., the peaks in Fig. 3(a), remarkable for the highest oscillator strength, are in the vicinity of the points $1+2s_6=2.305\,47$, $1+|s_5|+s_6=2.318\,13$, $1+s_6+s_7=5.918\,25$, $1+|s_5|+s_7=5.930\,91$, $1+s_6+\Omega_2=6.010\,63$, $1+|s_5|+\Omega_2=6.023\,29$, $1+|s_4|+|s_5|=6.118\,25$, $1+|s_2|+s_3=8.377\,78$, $1+|s_2|+\Omega_1=8.474\,19$, $1+|s_1|+|s_2|=8.572\,01$, $1+2s_7=9.531\,04$, $1+s_7+\Omega_2=9.623\,42$, $1+2\Omega_2=9.715\,80$, $1+|s_4|+s_7=9.718\,38$, and $1+|s_4|+\Omega_2=9.810\,76$. Again, analogously to the polaronic absorption, these resulting peaks can be thought of as a manifestation of transitions into relatively stable *relaxed excited states*[5] of a bipolaron. Analysis of these peaks leads to a conclusion that for the modes related to the *center-of-mass motions* in a bipolaron, the transitions to the scattering states involving the two-quantum excitations have, as a rule, oscillator strength one or even more orders of magnitude smaller than the transitions due to the one-quantum excitations.

All the other magnetoabsorption lines are revealed to be at the frequencies which are close to the combinations of the eigenfrequencies of a bipolaron in a magnetic field $|s_j|$ and/or Ω_J.

The oscillator strength of the absorption peaks assisted by many internal excitations of a bipolaron rapidly decreases with increasing number of quanta participating in the absorption process, when this number is high.

Even a small change of the magnetic field which corresponds to a shift of the electron cyclotron frequency from $\omega_c=0.20$ to $\omega_c=0.19$ makes *free polarons* to be the ground

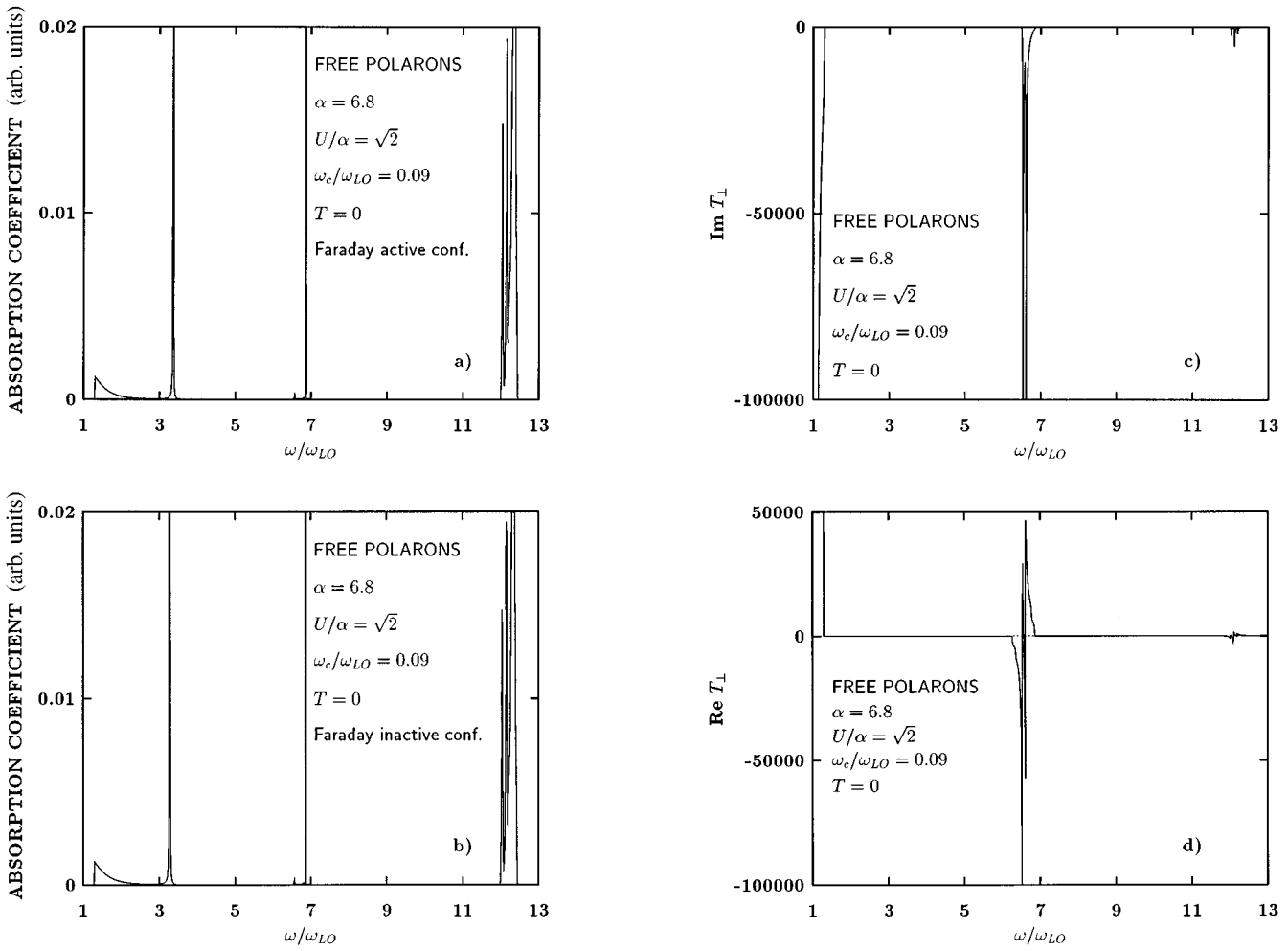

FIG. 6. Absorption spectrum of free polarons in a magnetic field for $\alpha=6.8$, $U/\alpha=\sqrt{2}$, and $\omega_c=0.09$ at $T=0$. Denotations are the same as in Fig. 3. The calculation was performed with the following eigenfrequencies of a larghe bipolaron model (45): $|s_1|=|s_4|=5.58$, $|s_2|=|s_5|=0.008$, $s_3=s_7=5.50$, $s_6\to 0$, $\Omega_1=\Omega_2=5.54$, and $\Omega_3\to 0$.

state of the system instead of the *bipolaron* state (see Fig. 2 and discussion at the beginning of the present section). Hence, this shift drastically changes the eigenfrequencies of the ground state of the absorbing system as compared to those of a bipolaron. Some of them become degenerate (namely, $|s_1|=|s_4|,|s_2|=|s_5|,s_3=s_7,\Omega_1=\Omega_2$), while the others tend to zero ($s_6\to 0,\Omega_3\to 0$). This results in the magnetoabsorption spectrum due to the free polarons, shown in Figs. 4(a) and 4(b) for the Faraday-active configuration and for the Faraday-inactive confuguration, respectively. This spectrum, investigated in depth in Ref. 15, manifests striking differences from the above-discussed bipolaron magnetoabsorption spectrum. For the sake of comparison, the imaginary and real parts of the memory tensor due to the free polarons are displayed in Figs. 4(c) and 4(d), correspondingly.

The first broad absorption peak in Fig. 4(a) corresponds to the scattering state of a free polaron with $1+|s_2|=1.016\,52$, and the many-quantum satellites, while the second narrow peak at $\omega=2.98$ can be presumably interpreted to be due to a relaxed excited state of a polaron. The next absorption peaks of free polarons are in the spectral regions *where there is no absorption due to bipolarons* [e.g., compare Figs. 3(a) and 4(a)]. Namely, the third broad peak originates from a set of numerous transitions assisted by the scattering states of a free polaron starting with $1+s_7=6.475\,55$, many-quantum transitions included. It is followed by the fourth narrow peak at $\omega=7.00$ which can be as above referred to a relaxed excited state of a polaron. Finally, the next series of three high-frequency absorption peaks starts with $1+2s_7=11.951\,10$.

If the magnetic field increases, so that the electron cyclotron frequency becomes substantially larger than $\omega_c^{\rm crit}$, the spectra of bipolaronic magnetoabsorption reproduce all the qualitative features which were discussed above; see, e.g., Figs. 5(a) – 5(d) for $\omega_c=0.3$. On the other hand, if the magnetic field decreases, so that the electron cyclotron frequency becomes much smaller than $\omega_c^{\rm crit}$, the spectra of magnetoabsorption due to free polarons also retain all the aforementioned qualitative features; see, e.g., Figs. 6(a)–6(d) for $\omega_c=0.09$.

Figures 7(a)–7(d) display a comparison of magnetoabsorption due to bipolarons for the Faraday-active configuration as well as related components of the memory tensor in a restricted spectral region for $\omega_c=0.2$ and $\omega_c=0.3$. They provide also evidence for the fact that the oscillator strength of the absorption peaks due to transitions to many-quanta scat-

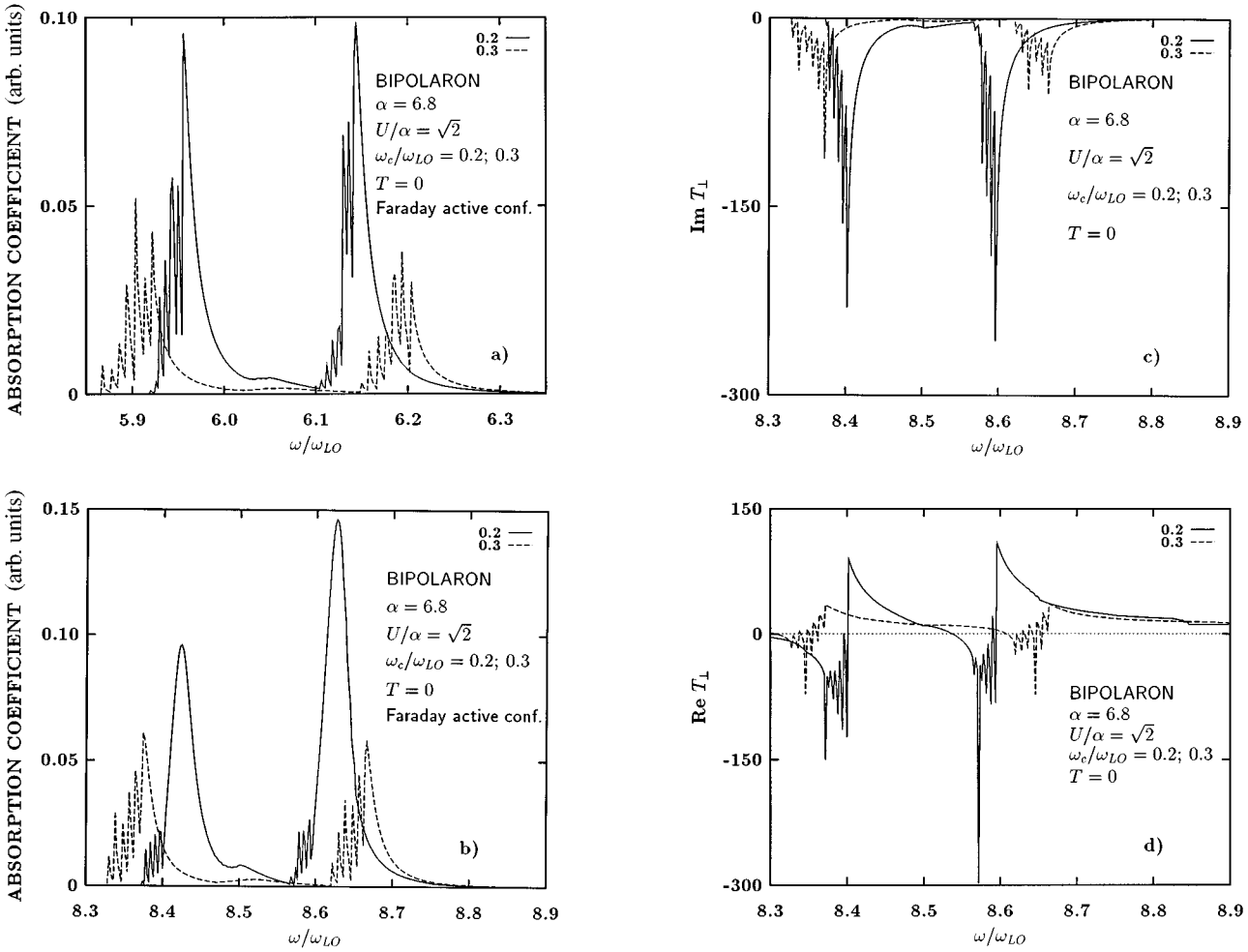

FIG. 7. Comparison of the detailed absorption spectra of a bipolaron in a magnetic field for $\alpha = 6.8$ and $U/\alpha = \sqrt{2}$ in the Faraday active configuration for $\omega_c = 0.2$ and $\omega_c = 0.3$ in two spectral regions: (a) $5.85 \leqslant \omega \leqslant 6.35$ and (b) $8.30 \leqslant \omega \leqslant 8.90$. For reference, in the latter case imaginary and real parts of the memory function are shown in panels (c) and (d), correspondingly.

tering states quickly decreases with increasing number of internal excitations of a bipolaron taking part in the absorption process, when this number is high. In such a way, a set of satellite sidebands of each peak due to the low-quanta transition appear.

Thus, we have shown that when the magnetic field is increased, a radical change of the magnetoabsorption spectrum shape occurs, namely, from that due to free polarons at lower magnetic fields (so that $\omega_c < \omega_c^{\rm crit}$) to another one specific for bipolarons at higher magnetic fields (when $\omega_c > \omega_c^{\rm crit}$). Such experiments on magnetoabsorption might give a crucial insight into the physics of large bipolarons in magnetic fields.

ACKNOWLEDGMENTS

Discussions with F. Brosens are gratefully acknowledged. This work has been supported by the E. E. C. Human Capital and Mobility Program ''Polarons, bipolarons and excitons. Properties and occurrences in new materials'' (Contract No. CHRX-CT93-0124; extension No. CIPD-CT94-0032) and N.F.W.O. Project Nos. G.0297.95, 113-1195, and the W.O.G. 0073.94N.

*Also at Universiteit Antwerpen (RUCA), Groenenborgerlaan 171, B-2020 Antwerpen, België and Technische Universiteit Eindhoven, P. O. Box 513, 5600 MB Eindhoven, The Nederlands.

†Permanent address: Department of Theoretical Physics, State University of Moldova, Strada A. Mateevici, 60, 277009 Kishinev, Republic of Moldova.

[1] J. T. Devreese, Polarons, in *Encyclopedia of Applied Physics*, edited by G. L. Trigg (VCH, New York, 1996), p. 383.

[2] R. P. Feynman, R. W. Hellwarth, C. K. Iddings, and P. M. Platzman, Phys. Rev. **127**, 1004 (1962).

[3] R. P. Feynman, Phys. Rev. **97**, 660 (1955).

[4] F. C. Brown, in *Polarons and Excitons*, edited by C. G. Kuper and G. D. Whitfield (Oliver and Boyd, Edinburgh, 1963), p. 323.

[5] J. T. Devreese, in *Polarons in Ionic Crystals and Polar Semiconductors*, edited by J. T. Devreese (North-Holland, Amsterdam, 1972), p. 83.

[6] V. L. Gurevich, I. G. Lang, and Yu. A. Firsov, Fiz. Tverd. Tela **4**, 1252 (1962) [Sov. Phys. Solid State **4**, 918 (1963)].

[7] E. Kartheuser, R. Evrard, and J. Devreese, Phys. Rev. Lett. **22**, 94 (1969).

[8] D. Larsen, in *Polarons in Ionic Crystals and Polar Semiconductors*, edited by J. T. Devreese (North-Holland, Amsterdam, 1972), p. 237.
[9] D. Larsen, in *Landau Level Spectroscopy*, edited by G. Landwehr and E. Rashba (North Holland, Amsterdam, 1991), Vol. 1, p. 109.
[10] E. Johnson and D. Larsen, Phys. Rev. Lett. **16**, 655 (1966).
[11] J. Waldman, D. M. Larsen, P. E. Tannenwald, C. C. Bradley, D. R. Cohn, and B. Lax, Phys. Rev. Lett. **23**, 1033 (1969).
[12] J. Vigneron, R. Evrard, and E. Kartheuser, Phys. Rev. B **18**, 6930 (1978).
[13] J. Van Royen, J. De Sitter, L. F. Lemmens, and J. T. Devreese, Physica B+C **81**, 101 (1977).
[14] J. Van Royen and J. T. Devreese, Solid State Commun. **40**, 947 (1981).
[15] F. M. Peeters and J. T. Devreese, Phys. Rev. B **25**, 7281 (1982).
[16] R. W. Hellwarth and P. M. Platzman, Phys. Rev. **128**, 1599 (1962).
[17] J. T. Marshall and M. Chawla, Phys. Rev. B **2**, 4283 (1970).
[18] R. Evrard, E. Kartheuser, and J. T. Devreese, Phys. Status Solidi B **41**, 431 (1970).
[19] Y. Lépine and D. Matz, Can. J. Phys. **54**, 1979 (1976).
[20] R. P. Feynman and A. R. Hibbs, *Quantum Mechanics and Path Integrals* (McGraw-Hill, New York, 1965), p. 308.
[21] F. Brosens and J. T. Devreese, Phys. Status Solidi B **145**, 517 (1988).
[22] V. M. Fomin and E. P. Pokatilov, Phys. Rep. **158**, 205 (1988).
[23] J. T. Devreese and F. Brosens, Phys. Rev. B **45**, 6459 (1992).
[24] F. M. Peeters and J. T. Devreese, Phys. Rev. B **34**, 7246 (1986).
[25] J. W. Hodby, G. Russell, F. Peeters, J. T. Devreese, and D. M. Larsen, Phys. Rev. Lett. **58**, 1471 (1987).
[26] J. T. Devreese and F. M. Peeters, in *The Physics of the Two-Dimensional Electron Gas*, edited by J. T. Devreese and F. M. Peeters (Plenum, New York, 1987), p. 131.
[27] R. J. Nicholas, M. Watts, D. F. Howell, F. M. Peeters, Wu Xiaoguang, J. T. Devreese, L. van Bockstal, F. Herlach, C. J. G. M. Langerak, J. Singleton, and A. Chery, Phys. Rev. B **45**, 12 144 (1992).
[28] N. Miura, H. Nojiri, and Y. Imanaka, in *Proceedings of the 22nd International Conference on the Physics of Semiconductors*, edited by D. J. Lockwood (World Scientific, Singapore, 1994), Vol. 2, p. 1111.
[29] P. Sigg, P. Wyder, and J. A. A. J. Perenboom, Phys. Rev. B **31**, 5253 (1985).
[30] J.-P. Cheng, B. D. McCombe, G. Brozak, and W. Schaff, Phys. Rev. B **48**, 17243 (1993).
[31] V. L. Vinetskii, Zh. Eksp. Teor. Fiz. **40**, 1459 (1961) [Sov. Phys. JETP **13**, 1023 (1961)].
[32] H. Hiramoto and Y. Toyozawa, J. Phys. Soc. Jpn. **54**, 245 (1985).
[33] J. Adamowski, Phys. Rev. B **39**, 3649 (1989).
[34] G. Verbist, F. M. Peeters, and J. T. Devreese, Solid State Commun. **76**, 1005 (1990).
[35] G. Verbist, F. M. Peeters, and J. T. Devreese, Phys. Rev. B **43**, 2712 (1991).
[36] F. Bassani, M. Geddo, G. Iadonisi, and D. Ninno, Phys. Rev. B **43**, 5296 (1991).
[37] A. S. Alexandrov and N. F. Mott, Rep. Prog. Phys. **57**, 1197 (1994).
[38] N. F. Mott, *Metal-Insulator Transitions* (Taylor & Francis, London, 1990).
[39] J. T. Devreese, G. Verbist, and F. M. Peeters, in *Polarons and Bipolarons in High-T_c Superconductors and Related Materials*, edited by E. K. H. Salje, A. S. Alexandrov, and W. Y. Liang (Cambridge University Press, Cambridge, England, 1995), p. 385.
[40] J. T. Devreese, V. M. Fomin, and F. Brosens, Solid State Commun. **96**, 613 (1995).
[41] K. K. Thornber and R. P. Feynman, Phys. Rev. B **1**, 4099 (1970).
[42] K. K. Thornber, Phys. Rev. B **3**, 1929 (1971).
[43] F. M. Peeters and J. T. Devreese, Phys. Rev. B **23**, 1936 (1981).
[44] V. M. Fomin and J. T. Devreese, Solid State Commun. **96**, 79 (1995).
[45] F. Brosens and J. T. Devreese, Solid State Commun. **96**, 133 (1995).
[46] W. B. da Costa and F. M. Peeters, J. Phys. Condens. Matter **7**, 1293 (1995).